DOI: 10.15480/882.9322

Eighth International Symposium on Marine Propulsors
smp'24, Berlin, Germany, March 2024

Numerical and experimental study of a series of contrarotating propellers

Jahn Terje Johannessen[1], Lucia Sileo[2], Kourosh Koushan[2], Vladimir Krasilnikov[2], Simon Froitzheim[3], Reinhard Schulze[3]

[1]Brunvoll, Norway
[2]SINTEF Ocean, Trondheim, Norway
[3]Schiffbau-Versuchsanstalt Potsdam GmbH, Germany

ABSTRACT

The authors conducted development and analyses of a new series of contrarotating propellers (CRP) as part of a research project funded partly by the Norwegian Research Council and led by the propeller manufacturer Brunvoll. The paper describes the initial investigation for choosing the design matrix, method used for the design of the propeller geometries, potential and CFD based numerical analyses, and open water as well as cavitation model experimental investigations.

The main idea behind this new series is to utilize the capability that rate of revolution of the fore and aft propellers can be adjusted independently providing more operational flexibility and better overall efficiency over a wide range of operational conditions. Initial designs were performed using a numerical tool based on potential flow; however, some designs were refined based on analyses performed using CFD. A set of propellers were tested both at SINTEF Ocean and SVA Potsdam. The paper presents the methodology used for the design as well as numerical and experimental investigation of this series. Results are provided graphically. Comparison between results from different numerical methods and the model tests are shown and possible deviations are discussed.

Keywords

Contrarotating propellers, potential methods, CFD, model tests.

1 INTRODUCTION

Contra Rotating Propeller (CRP) for ships is an invention known from the 19th Century. This propulsion system recovers part of the slipstream rotational energy, which is lost with single propeller configuration, and thereby enhances the hydrodynamical efficiency.

For the design of CRP, the results of model tests are often used. Results and documentations of those are given by several authors, such as Kracht et al. (1971), Kracht (1976), van Manen and Sentic (1956), van Manen and Oosterveld (1968) and Oosterveld (1971).

The first significant model tests with CRP were carried out in 1956 in Wageningen by Manen and Sentic (1956). A number of 3-bladed propellers of the type Wageningen B were assembled. The propeller geometries were not optimal and van Manen and Oosterveld (1968) published the first important series of contra-rotating model propellers. The CRPs were designed in Wageningen according to the lifting line theory. The pitch distributions of the propellers have uniform tendencies. Front and rear propellers show the maximum pitch at $r/R = 0.7$ and the tip and hub are slightly unloaded.

A series of 4 CRPs was investigated at the SSPA in the years 1965 - 1968 by Bjärne (1973). They were designed for the range of fast container ships to full tankers based on a modified lifting line design theory for CRP by Lerbs. The efficiencies of this series are lower than those of comparable Wageningen B propellers.

Kracht (2000) analyzed the design parameters of CRP. The main parameters of the front and rear propeller are the same as of a single propeller. Also, the influence of the main parameters on the propeller characteristics is similar.

The blade numbers are usually different to avoid vibrational problems and the aft propeller diameter is smaller in order to stay within the slip stream contraction from the forward propeller.

The horizontal distance between the generator lines of both propellers has a major influence on the characteristics of both propellers including the force and torque fluctuations.

Also, the parameters of ideal propellers are influenced by the horizontal distance as published by Kracht (1976), (2000) and Beveridge (1974). The pitch ratio of the front propeller will decrease with growing propeller distance, while the pitch ratio of the rear propeller is increasing, and the diameter is simultaneously decreasing. Schmidt (2000) carried out systematic tests with a variation of the propeller distance for the development of thrusters and podded drives with contrarotating propellers at SVA Potsdam.

CRPs are found in a high number of applications, but mainly for small high-speed outboard units with Z-drive gearboxes. However, there are considerable technological barriers in making long shaft lines for CRP, and complicated mechanical design is most likely one of the main reasons for CRP not being frequently used in merchant ships.

Brunvoll developed and delivered a CRP main propulsion system driven by two permanent magnet (PM) motors for the platform supply vessel M/S Juanita. This installation has functioned well since she came into operation in 2014 and the feedback from the ship owner on functionality and fuel consumption is positive. According to ship owner Ugland Offshore, the fuel consumption at service speed (14,0-14,5 kn) for Juanita is 19 % lower than for the sister ship. The gross tonnage of Juanita is also 14 % higher than Evita.

2 INNOVATIONS AND ADVANTAGES

Brunvoll is up to date the only supplier globally which has delivered a CRP propulsion system for commercial ship with direct drive, using electrical PM motors on a single shaft line. There is considerable interest from the market regarding CRP for main propulsion, but industrializing this propulsion concept is a big challenge, and there are two main reasons for this. First the mechanical and hydraulic concept for long contrarotating shaft in shaft solutions are very demanding and involve significant risk, created by too high investment and maintenance cost compared to fuel savings. Second, CRP is hydrodynamically highly complex, and more knowledge is needed about hydrodynamic design features to produce optimal propeller design.

The Brunvoll solution with use of two separate electrical motors allows for propellers to be run on independent rpm's and thereby it is possible to optimize efficiency by individual control of rpm. Other solutions, with a separate propeller mounted in a steerable pod behind the main propeller, will need installation of two separate propulsion units, thereby increasing cost and complexity. Accordingly, a solution with a steerable unit will put restriction on minimum distance between propellers due to the need for turning the aft propeller as a rudder. This will limit possibilities for hydrodynamically optimizing the distance between the propellers.

CRP for shaft line can also be installed as multiple screw in a ship. Resistance for ship hulls designed for single screw propulsion is normally lower than the resistance for hulls with two or several screws. Additionally, for single screw ships, the propulsion efficiency factors are considered advantageous. This is due to the location of the propeller in the wake field behind the bulb part of the stern. This gives additional efficiency gain to ships that can replace twin screw solutions with CRP system, and still comply with redundance requirements. Limited space for propeller diameter is a common restriction in merchant ship design, and it is therefore usual to be forced to choose smaller propeller diameter than optimum. The optimum diameter of a CRP is however smaller than for a single propeller, and selecting CRP system will thereby make it possible to select propellers that are closer to optimal diameter than single propeller systems, thereby contributing to enhanced propulsion efficiency.

The CRP system is very compact, and it is therefore also a suitable solution for retrofit projects. The global ship sector is responsible for a significant part of greenhouse gas emissions as well as noise pollution in the ocean. Industrializing the CRP is expected to have a positive effect on both reducing air pollution and noise pollution into the sea. Many ship types are relevant for CRP. The efficiency gain is expected to be highest for ships with large portion of time spent in transit, but CRP can be valuable for other ship types as well. The global technology shift towards electrification and hybrid systems is also supportive to the introduction of CRP with electrical motors.

3 SETUP OF THE SERIES

A series, specifically for CRP systems with a free rate of revolution for each propeller on a single shaft line was needed. With the series, the selection of an ideal CRP for an arbitrary case should be possible. Therefore, the series should cover the whole range of use cases, where a CRP-system gives the designer an advantage over other propulsion systems such as a single propeller or a ducted propeller. Since C_{TH} is the parameter, that defines a reasonable usage (Figure 14) of a CRP in the best way, it was clear from the beginning, that this parameter should define the first dimension of the newly developed CRP – series.

To calculate the respective C_{TH} for a specific CRP system, which shall be selected with the series, the total thrust T, the diameter of the respective front propeller D_{FWD} and the inflow speed V_A must be known, since C_{TH} is defined as follows:

$$C_{TH} = \frac{8\,T}{\rho\,V_A^2\,D_{FWD}^2\,\pi} = \frac{8}{\pi}\cdot\frac{K_T}{J^2} \qquad (1)$$

This is generally the same approach as used for example for the selection of propellers from the Wageningen B – Series, where K_T/J^2 is calculated.

In the Wageningen B – Series, propellers with different pitches are collected. P/D is therefore on the second axis. By comparing the open water efficiency of the different pitched propellers at a certain K_T/J^2 value, the ideal propeller can be selected. Advantage of this procedure is, that a fitting and efficiency wise good propeller for an

arbitrary rate of revolution can be selected. The disadvantage is, that the propellers are not designed for the selected operating point. The aim of the present series is a different one. On the one hand, the rate of revolution is not restricted because the rate of revolution can be adjusted independently for every propeller. The use of electric engines gives much more freedom to choose the propellers rates of revolution. On the other hand, design propellers with reasonable cavitation behavior shall be the result of a propeller selection with the series. Therefore, not a pitch variation was selected to get a second axis, but a different approach was used. To populate the series only with design propellers, it is necessary to define operating points in a unique way for every point of the series. A constant C_{TH} can be achieved by endless combinations of the three input parameters T, D_{FWD} and V_A. This results in the need to fix one of the three parameters and put one of the others on the second axis of the series. This results in the fact, that there is no possibility to generate dimensionless expressions on the second axis, since all applicable standard non-dimensional values include result values (such as n_{FWD}).

The decision was made to set up the whole series for a front propeller diameter of D_{FWD} = 1 m and to use the propeller thrust, calculated for a propeller of D_{FWD} = 1 m on the second axis of the series. Since this is not a dimensionless parameter [N], upper, and lower boundaries were defined in respect to the available ship database of SVA Potsdam.

With these expressions selected for the two dimensions of the series, the series covers all relevant operating points in the range from C_{TH} = 0.7 to C_{TH} = 4.0. Therefore, design CRP propellers with a unique and cavitation optimized geometry can be designed for all points of the series.

The selection of a propeller generally follows a similar procedure to the selection of a propeller from the Wageningen B -Series. For a certain ship application, the C_{TH} is calculated. Instead of selecting the propeller with the best efficiency or the one with the pitch resulting in the right rate of revolution at the given C_{TH} (respectively K_T/J^2), we select the CRP, which is designed for the right thrust. Next to the two propeller geometries, the rates of revolution and the rate of revolution ratio between the 2 CRP are part of the result of the selection.

For all 9 operating points of the matrix grid (Figure 1), a CRP system was designed including cavitation properties as well as reasonable wake fractions. The cavitation numbers as well as the wake fractions for each design point result from a regression model from the SVA Potsdam database.

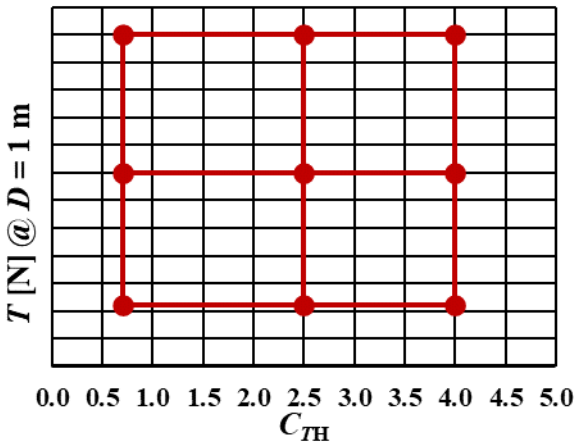

Figure 1 Schematic presentation of the matrix

4 EXPERIMENTS

Experimental methods and set up were developed for evaluations of contrarotating propellers in open water condition. Model tests of some design pairs were performed in the towing tanks of SINTEF Ocean and SVA Potsdam. Cavitation tests of couple of pairs of contrarotating propellers were conducted in the cavitation tunnel of SVA Potsdam.

4.1 Set-up for the tests in the towing tank

The tests in the towing tank were performed in several steps. For the open water test with the forward propeller alone, standard open water setup was used using H29 open water dynamometer as presented in Figure 2. In these tests the propeller is run in pulling mode. The gondola strut is then on the pressure side of the propeller. The cap shown in Figure 2 is then attached and rotating with the propeller on the suction side. On the pressure side there is a cone mounted fixed to the H29. This cone is not rotating and has a gap of 1.5 mm to the propeller boss on pressure side.

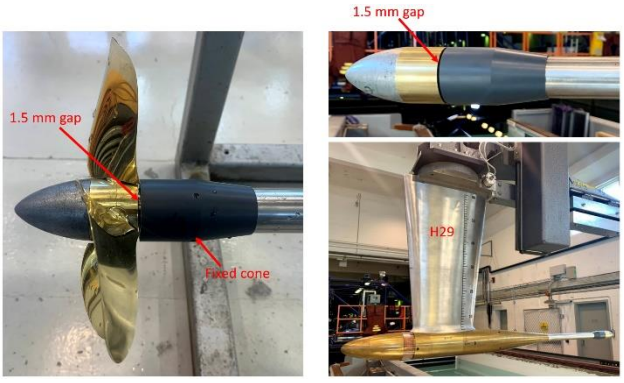

Figure 2 Set-up for open water tests

For the contra rotating setup, a customized rig was designed and manufactured. In the contra rotating mode, the forward propeller is mounted on H29 propeller dynamometer in pushing mode (strut of gondola is on the suction side) and the aft propeller is mounted on H39 open water dynamometer (strut of the gondola is on the pressure side). Cones fixed to the gondolas are mounted on the pressure side of the aft propeller and on the suction side of

the forward propeller. The cones have 1.5 mm gap to the bosses. The cones will not rotate with the propellers. Flat caps are used in this mode. Caps are rotating with the propellers. There is 1.5 mm gap between the caps. Contra rotating setup is shown in Figure 3.

Propeller shaft submergence was 42 cm during all tests.

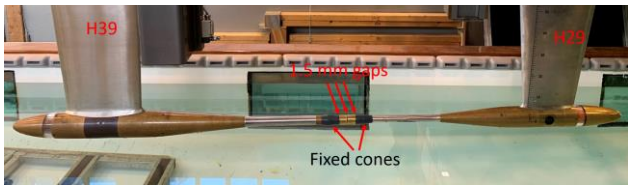

Figure 3 CRP open water test set-up

4.2 Analysis and results of the tests in the towing tank

To analyze the results of open water tests with contra rotating propellers a set of coefficients are used for the forward, the aft and the CRP. **Fehler! Verweisquelle konnte nicht gefunden werden.** Table 1 shows definition of the coefficients that are used. These coefficients are in line with the ITTC guideline on "Hybrid Contra-Rotating Shaft Pod Propulsors Model Test" 7.5.-02-03-01.6 (ITTC 2017a). All coefficients for single propellers are based on the rate of revolution and diameter of the forward propeller. Efficiency of contra rotate ng system is calculated based on the total power required to drive both forward and aft propellers. Subscription FWD refers to the forward propeller, subscription AFT to the aft propeller and subscription CRP to the contra rotating system (both propellers).

Table 1 Coefficient used for analyzing the test results

$$J_{corr} = \frac{V_A}{n_{FWD} \cdot D_{FWD}} - \Delta J$$

$$K_{TFWD} = \frac{T_{FWD}}{\rho \cdot n_{FWD}^2 \cdot D_{FWD}^4}$$

$$K_{TAFT} = \frac{T_{AFT}}{\rho \cdot n_{FWD}^2 \cdot D_{FWD}^4}$$

$$K_{QFWD} = \frac{Q_{FWD}}{\rho \cdot n_{FWD}^2 \cdot D_{FWD}^5}$$

$$K_{QAFT} = \frac{Q_{AFT}}{\rho \cdot n_{FWD}^2 \cdot D_{FWD}^5}$$

$$K_{TCRP} = K_{TFWD} + K_{TAFT}$$

$$K_{QCRP} = K_{QFWD} + \frac{n_{AFT}}{n_{FWD}} K_{QAFT}$$

$$\eta_{CRP} = \frac{\left(T_{FWD} + T_{AFT}\right) \cdot V_{corr}}{2\pi \left(n_{FWD} \cdot Q_{FWD} + n_{AFT} \cdot Q_{AFT}\right)}$$

$$\eta_{CRP} = \frac{J_{corr}}{2\pi} \frac{K_{TCRP}}{K_{QCRP}}$$

Since the forward propeller is working in pushing mode in contra rotating setup, then the velocity seen by the propeller must be corrected by the wake of the gondola in front of the forward propeller. This correction ΔJ is found by running the forward propeller first in pulling mode, then in pushing mode (with the aft gondola present) and using thrust identity. Figure 4 presents as an example the advance coefficient as function of K_T when the propeller is running at 10 Hz. Open water test is then performed both in pulling and pushing mode. The difference in J is calculated for the same K_T. This difference is denoted ΔJ, which is then used to correct the J value during tests in CRP configuration due to the fact the flow is slightly blocked by the propeller dynamometer gondola. The correction is small as can be seen from the data presented in Figure 4.

Tests were conducted with several sets of contra rotating propellers at different pitch ratios and different loading distribution between the forward and aft propellers. Change of loading distribution between the forward and aft propellers were done by keeping the forward propeller rate of revolutions constant and adjusting the aft propeller rate of revolution. As an example, Figure 5 shows a set of propellers that were tested at 5 different loadings. Thrust coefficient, torque and efficiency of the contra rotating system (both forward and aft propellers together) are presented as function of corrected advance coefficient. Rate of revolution and diameter of forward propeller is used as reference when calculating these coefficients. Forward propeller rate of revolutions is kept at 19 Hz while aft propeller rate of revolution is 21.422 Hz as basis, but also variations of aft propeller rate of revolutions of ±5% and ±10% are tested.

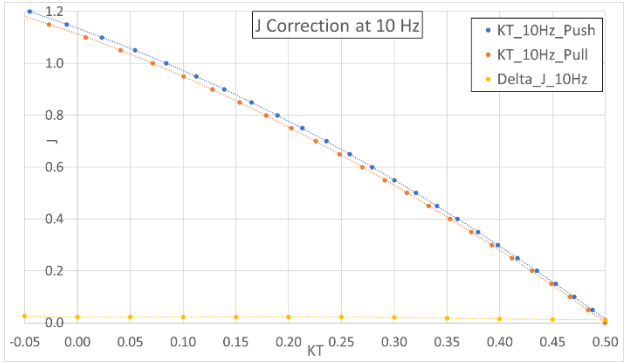

Figure 4 Advance coefficient correction based on thrust identity

A higher rate of revolutions of the aft propeller leads to higher loading ratio of the aft to the forward propeller and lower rate of revolutions of the aft propeller leads to lower loading ratio of the aft to the forward propeller. As the loading on the aft propeller is relatively increasing, then higher thrust and torque coefficients are measured for the same advanced coefficient. The maximum efficiency is not changed substantially by changing the loading ratio between the aft and the forward propeller, but the advance

coefficient at maximum efficiency is smaller for lower loading ratio between the aft and the forward propellers.

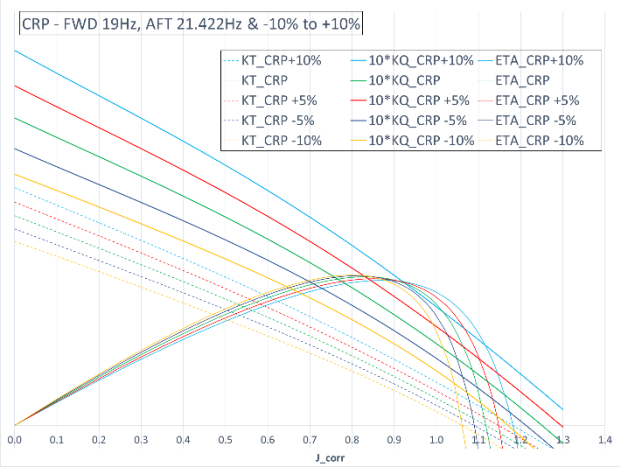

Figure 5 CRP open water diagrams for different aft propeller rate of revolutions

Open water test results can be also presented as function of propeller loading coefficient C_{TH}. This is presented in Figure 6 for the open water test results presented in Figure 5. For this set of propellers, maximum efficiency is reached around thrust loading coefficient of 1. It is observed that different efficiency curves, which represent different loadings, as a function of thrust loading coefficient are almost identical. This is also proof of measurement accuracy. Slight differences are observed close to maximum efficiency. Lower loading leads to slightly better maximum efficiency. As expected, higher loading leads to higher thrust and torque coefficients.

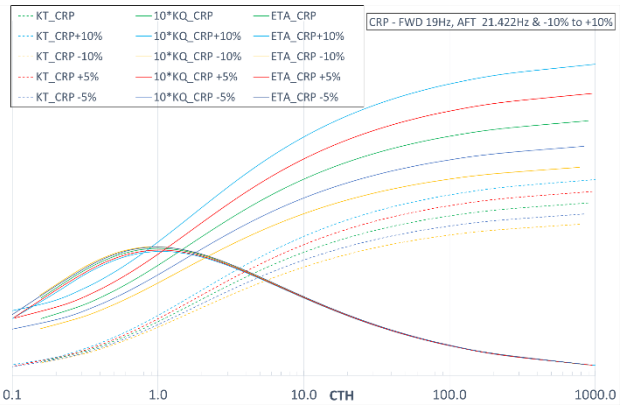

Figure 6 Performance of CRP as a function of thrust loading coefficient at different aft propeller rate of revolutions

Figure 7 shows thrust and torque coefficients of forward propeller at three different aft propeller loadings. Both thrust and torque coefficients of forward propeller are getting larger when the aft propeller loading is decreased. This shows that also the aft propeller is affecting the performance of the forward propeller.

Figure 8 presents the thrust and torque coefficients of the aft propeller for different loadings achieved by adjusting the rate of revolutions of the aft propeller, while keeping the rate of revolutions of the forward propeller unchanged. Both thrust and torque coefficients are increasing with higher loading.

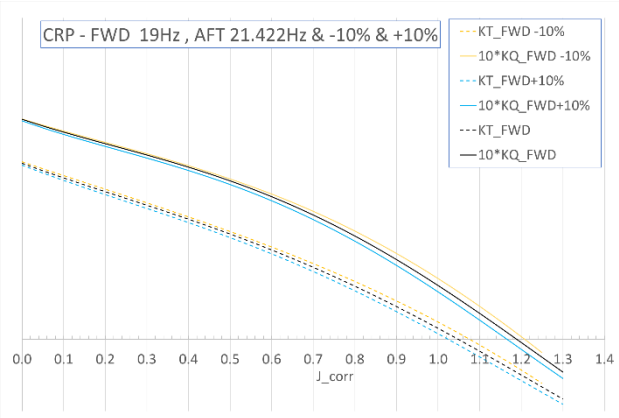

Figure 7 Thrust and torque coefficients of the forward propeller at different rate of revolutions of the aft propeller

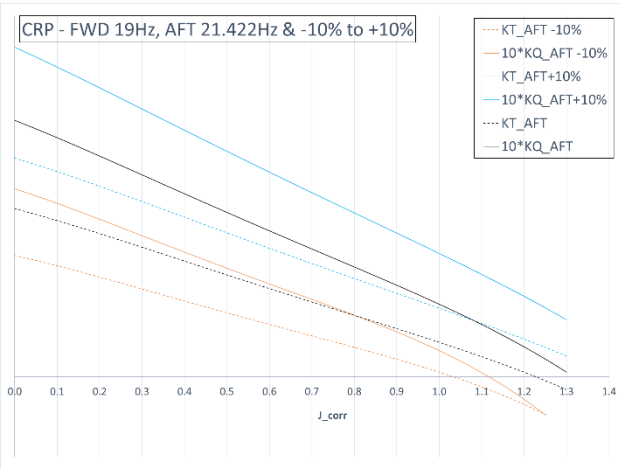

Figure 8 Thrust and torque coefficients of the aft propeller at different propeller rate of revolutions of the aft propeller

4.3 In the tunnel

The cavitation tests for an exemplary CRP system were carried out in SVA Potsdam's Cavitation tunnel K15A of Kempf & Remmers. The cavitation behavior of the CRP on a single shaft line was observed while the propellers were running at different rate of revolution at the design point and at over and under load condition in the axial design wake field as well as in homogeneous inflow. In this paper only an excerpt of the results is presented. The cavitation was filmed with a high resolutions high-speed camera to cover the cavitation at both propellers simultaneously. This cannot be done with the use of a strobe and a normal camera due to the different rate of revolutions of the propellers.

The axial design wake field was simulated by wire screens and was measured by LDV according to "Model – Scale Cavitation Test" 7.5 – 02 03-03.1 (ITTC 2017b). Figure 9 shows the good match between the target w and measured wake at the most relevant relative radius $r/R = 1$.

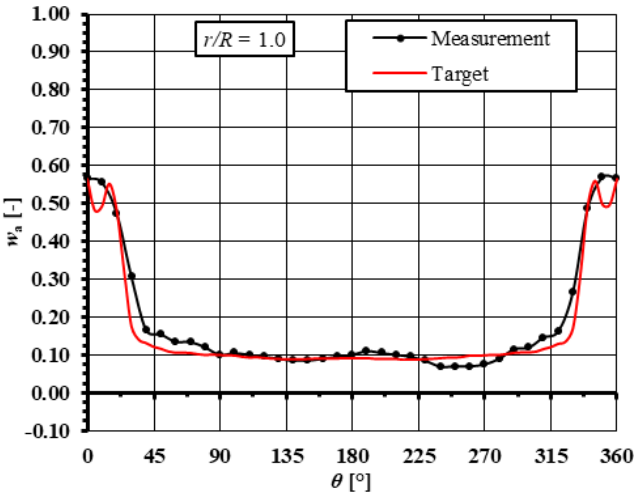

Figure 9: Axial wake field at *r/R* = 1, target and LDV measurement

In this paper, exemplarily, the design point of the CRP as well as a hypothetical operating point at a significantly lower cavitation number are presented. The cavitation number is defined as follows:

$$\sigma_n = \frac{p_A - p_V + \rho \cdot g \cdot h_0}{0.5 \cdot \rho \cdot n^2 \cdot D^2} \qquad (2)$$

Table 2: Presented operating points in the cavitation tests

OP	n_{FWD}	$K_{T\text{-FWD}}$	$K_{T\text{-AFT}}$	$\sigma_{n\text{-FWD}}$	
[-]	[rps]	[-]	[-]	[-]	
1	19	0.1465	0.2176	7.50	Design Point
2	19	0.1465	0.2176	3.50	Low σ_n

Table 2 presents different operating points for the cavitation tests. For the CRP design point OP1, the front propeller shows a very small region of rarely appearing intermittent tip vortex cavitation at the blade, which develops into a thin detached tip vortex in the propeller wake when the propeller rotates. This behavior sometimes can be seen in the peak of the wake field (approx. Θ = 0° - Θ = 30°). In the region of the aft propeller, this tip vortex sometimes reappears if the aft propeller is in the respective position. When a blade of the rear propeller is moving through the peak of the wake field (approx. Θ = 0° - Θ = 40°), in low percentage of the cases a rarely occurring intermittent tip vortex is visible, which develops into a thin attached tip vortex. For about the same percentage, no attached tip vortex can be seen at all, and the tip vortex appears only in the wake. Most of the time no tip vortex is present. Both pressure sides are free of cavitation.

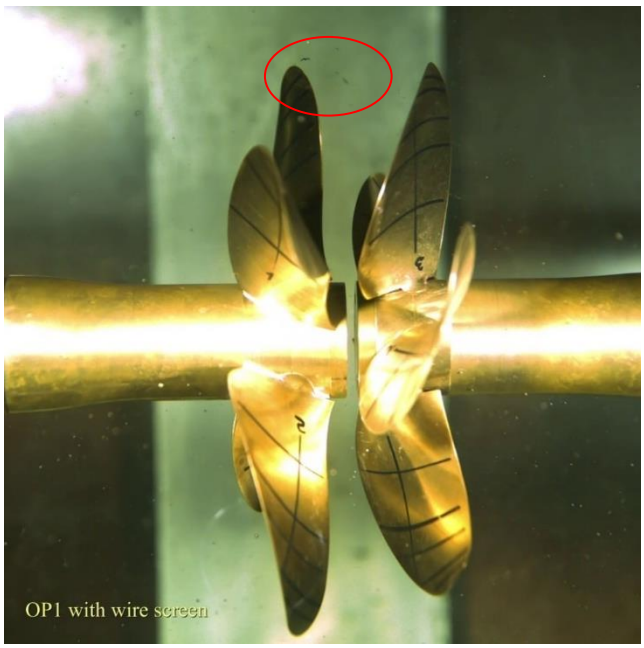

Figure 10: Cavitation photograph, OP1 with wake, focus on front propeller, port side view

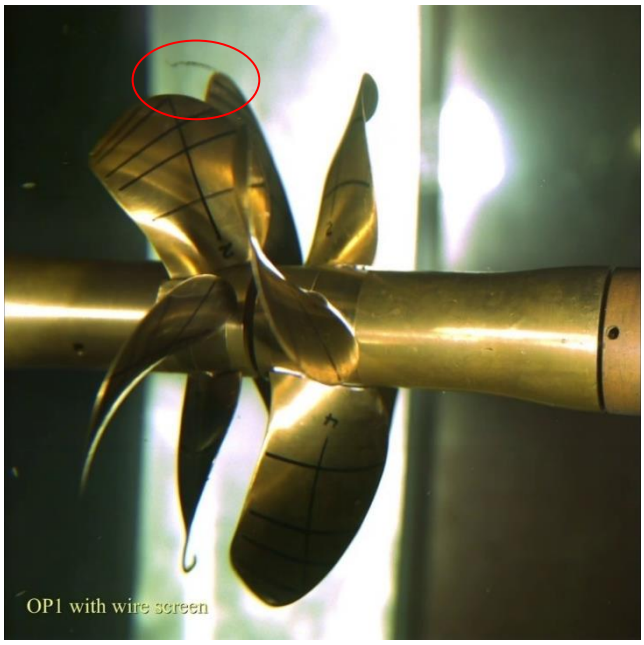

Figure 11: Cavitation photograph, OP1 with wake, focus on aft propeller, star board view

OP2 is a hypothetical operating point to see how the cavitation would develop at lower cavitation numbers. At the front propeller sheet cavitation covers the suction side side from *r/R* = 0.90 to *r/R* = 0.95, when moving through the wake peak (approx. Θ = 0° - Θ = 40°). The sheet cavitation develops to tip vortex cavitation. At the aft propeller attached tip vortex cavitation is present in the peak of the wake field. In the range from (approx. Θ = 20° - Θ = 40°) the aft propeller is hit by the cavitating tip vortex of the front propeller at *r/R* = 0.95, which leads to a local cloud cavitation. The tip vortices of front and aft propeller interact in the propeller wake and dissipate fast. Both pressure sides are free of cavitation.

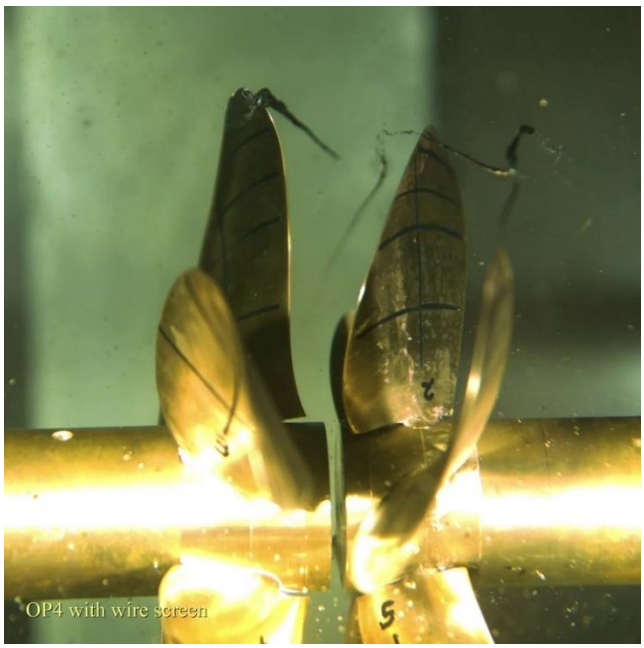

Figure 12: Cavitation photograph, OP2 with wake, port side view

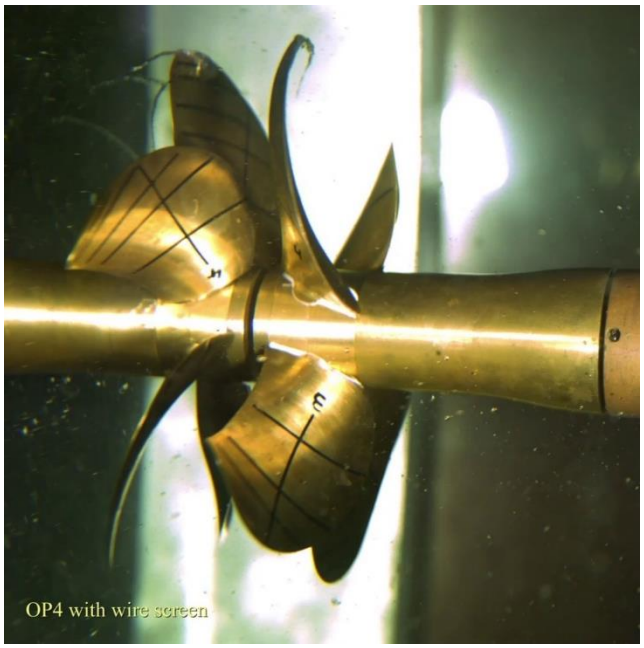

Figure 13: Cavitation photograph, OP2 with wake, star board view

5 NUMERICAL INVESTIGATIONS

Numerical calculations of all propeller configurations were performed using a potential flow theory-based tool, some configurations were analyzed using the CFD Software STAR CCM+.

The calculation and design process was divided into several stages. Initial estimations of the behavior of contrarotating propellers, arranged closely behind each other, can already be obtained from impulse theory considerations. This applies, for example, to the diameter ratio of the two propellers. The jet contraction of the wake field of the front propeller can be taken into account by means of simple estimation methods.

This is illustrated in Figure 15 as a function of the diameter ratios.

5.1 Predesign and potential methods

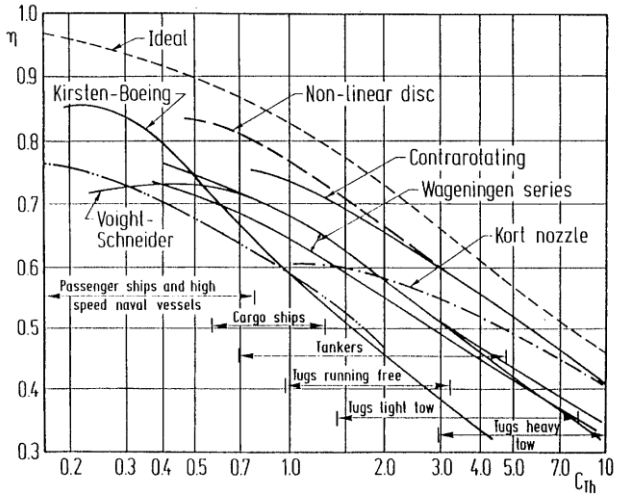

Figure 14: Presentation of empirical values with efficiencies of different propulsion systems, (Breslin et al. (1994))

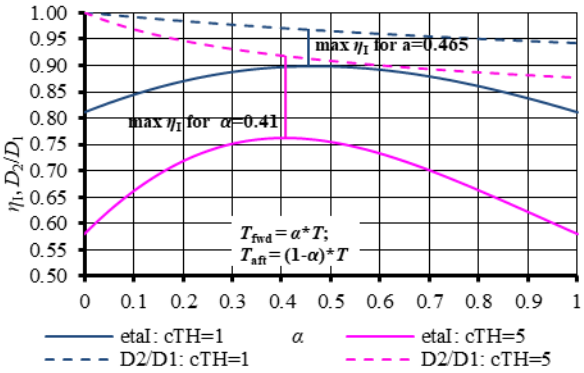

Figure 15: Optimal diameter ratios for a CRP system derived from momentum theory (ideal efficiency)

In a next step, a more detailed estimation of the best possible combination of the respective blade numbers, diameters and other propeller main parameters can be determined on the basis of Wageningen polynomial coefficients (van Lammeren et al. 1969, Oosterveld et al 1975). The effect of the front propeller on the rear propeller is measured by a shift of the advance coefficient for the rear propeller. This change of the advance coefficient for the rear propeller is substantially dependent on the thrust loading coefficient C_{TH} of the front propeller. Since the wake of the front propeller contains not only axial velocity components, but also tangential components, these can be approximated by a virtual change of the rate of revolution for the rear propeller. To ensure that the slight suction effect on the front propeller caused by the rear propeller is also included, a small change in the advance coefficient and rate of revolution for the front propeller is also taken

into account in this procedure. However, this interaction can only be realized through an iterative approach. The induced velocities (axial and tangential) are approximated by the use of empirical formulas.

SVA Potsdam has its own potential propeller calculation software VORTEX. VORTEX implements a vortex-lattice method. This class of methods takes into account all important geometrical variables (Schulze 2019). Based on the calculation methods related in VORTEX, an inverse method for determining an optimal propeller geometry was implemented using an optimization tool.

The definition of an evaluation criterion f(G): f(G) = f(G, J^* ,$\eta_O(J^*)$, $\sigma_n(J^*)$, $K_Q(J^*)$) is realized in such a way that f(G) is minimal, if $\eta_O(J^*)$ is maximal, $\sigma_n(J^*)$ minimal and $K_Q(J^*) = K_Q^*$, with predefined J^* and K_Q. J^* represents the respective design advance coefficient of the propeller, while for example K_Q^* represents the K_Q corresponding to this advance coefficient.

$\eta_O(J^*)$, $\sigma_n(J^*)$, $K_Q(J^*)$ can be calculated with an „arbitrary“ propeller calculation code. The propeller geometry is defined by a finite set of real numbers derived from a polynomial representation of the radial distributions of pitch, camber, skew and rake.

There are various algorithms available for solving the minimization problem such as Newton-like algorithms (Davidson-Fletcher-Powell) as well as direct-search-algorithms (Gablonski-algorithm).

These methods are realized in the SVA propeller code VTXopt (Schulze 1997) with the main tools of the program package VORTEX.

VTXopt is defined in such a way, that a multi objective optimization is possible. This is represented in Figure 16. For different advance coefficients different restrictions can be defined.

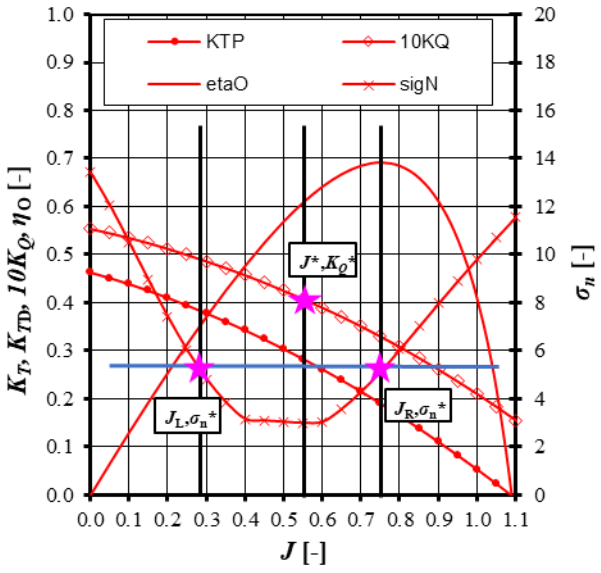

Figure 16: Multi objective optimization of the open water characteristic of a propeller, example

The consideration of the reciprocal interaction between the propellers is in principle carried out as previously described. Thus, the front and rear propellers are optimized individually, taking into account the axial and tangential induced speeds. The induced axial velocity components of the respective other propeller are taken into account by shifting the advance coefficient with respect to the velocity. The tangential induced velocity components are detected by a virtual change rate of revolution. Of course, this virtual change in speed also has an influence on the advance coefficient. Different to the above explained approach with the use of the Wageningen series to estimate and optimize the CRP characteristics, the induced velocities are here calculated with VORTEX at the respective propeller plane of the other propeller. The reciprocity of this influence by both propellers again requires an iterative approach. With reference data from model tests or representative CFD calculations available, additional corrections can be applied to increase the accuracy of the results.

5.2 CFD

Numerical studies based on a Reynolds Averaged Navier-Stokes (RANS) equation solver and experimental measurement to investigate the characteristics of CRP systems are not very common. Paik et al. (2015) investigated the wake characteristics of CRP using Stereoscopic Particle Image Velocimetry (SPIV) and RANS simulations. In Nouri et al. (2018), a RANS-based CFD tool, together with genetic algorithm, was used for optimizing a marine CRP.

In the present work, RANS simulations were first used to provide propulsive coefficients and to perform an initial wake adapted design of the CRP. After that, unsteady and blade-resolved RANS simulations of different CRP designs were performed and validated against model test data. The numerical investigations not only helped in having a better understanding of the complex phenomena involved in CRP, but provided the data to fill into the design matrix for the cases which were not tested experimentally.

5.2.1 Numerical setup

StarCCM+ (vers.17.02.007), based on the Finite Volume Method with a segregated flow solver, was used by SINTEF Ocean to simulate the incompressible turbulent flow past the CRP, at model scale, as tested in the SINTEF Ocean and SVA test campaigns and, for some cases, at full scale. This software contains a multi-regions part-based meshing setup, with different motion modelling capabilities. The fully resolved blade model of the CRP unit was analyzed in the CFD simulations with the Sliding Mesh (SM) approach to account for the rotation of the two propellers. The k-ω SST (Menter Shear Stress Transport) turbulent model was adopted for the full-scale simulations, where the fully turbulent assumption can be applied, while at model scale simulations the transition from laminar to turbulent was investigated, adopting the Gamma-Re-theta transition model. Simulations did run on 480 cores on the

SINTEF HPC Unity and about 20 hours of CPU hours were needed for completing 10 revs of simulation time. Four advance coefficient (J) values were considered for filling each open water curve.

The simulation setup includes an infinite cylindrical shaft in an open water domain, which means that it does not include the strut/gondola/cone configuration adopted in model tests. Nevertheless, the gaps between the FWD and AFT propellers and the shaft were kept. They were corresponding to 1.5 mm at model scale and 20 mm at full scale. A sketch of the computational domain and a generic geometrical model of the CRP unit are illustrated in Figure 17, while the CRP unit configuration with the two propellers and gap is illustrated in Figure 18.

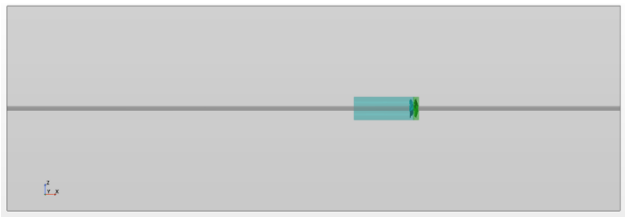

Figure 17 Computational domain for the CFD simulations

The diameter of the front (forward) propeller is the reference length, called here D. The external computational domain is a box with a frontal section of 10Dx10D and a total length of 30D (10D in front of the front propeller plane and 20D downstream). The sides of the domain are all defined as inlet boundaries except for the exit (downstream) side, where the pressure outlet boundary condition is imposed. The trimmed mesher from StarCCM+ was used to generate hexahedral based grid in the computational regions.

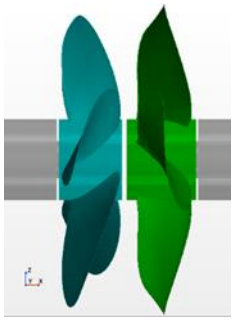

Figure 18 CRP configuration with gaps

Figure 19 Volume mesh on the blade surface wall

In the propeller regions the wall boundaries, corresponding to the blades and hubs, are defined as no-slip smooth walls. The cell size on the blades is about 1% of D, while higher resolution is needed along the leading edge and on the tip and TE area to properly define the main features of the blades, as shown in Figure 19.

Ten layers of prismatic cells are attached to the no-slip walls, to correctly capture the viscous effects in the boundary layer. The first cell height is defined so to have y+ larger than 70 at full scale and in the range 1-5 at model scale, as depicted in Figure 20.

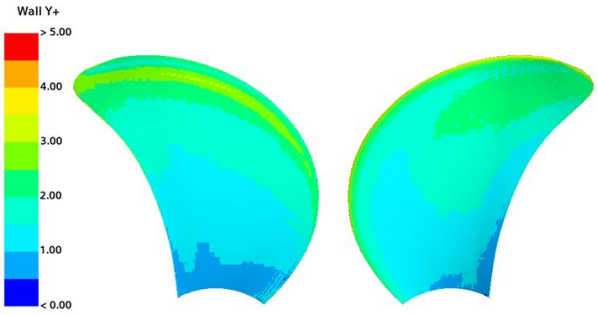

Figure 20 Wall y+ distribution on blade wall at MS

The time step is selected so to correspond to 2 degrees of rotation of the front propeller.

Integral values of thrust and torque on both propellers and their averaged values were calculated in the last 2 revolutions, and then compared against the experimental data, for the conditions that were investigated during the model test campaigns. For some specific conditions scale effects were also studied, carrying out the simulations at full scale in addition to the model scale.

5.2.2 Variation of RPM ratio on the SOBC-1 initial design.

Some preliminary CFD simulations were carried out on the SINTEF Ocean Bulk Carrier model (SOBC-1), whose characteristics and operational point were well suited as target ship for the CRP design. Resistance and propulsion simulations were performed to provide information about towing resistance, propulsion factors, nominal and effective wake, which were later used in the design of the CRP. Those simulations are not described here in detail. They were carried out using the same commercial software used for the CRP in open water conditions, StarCCM+, but the Actuator Disc (AD) was used in the self-propulsion case together with the SINTEF Ocean in-house propeller code, AKPA.

The obtained basic design of the CRP for the SOBC-1 case was investigated both experimentally and numerically by CFD. The comparison against model tests data was very important for validation of results and verification of the numerical strategy adopted in the following CFD simulations. Mesh sensitivity studies were performed on this initial CRP design, and special attention was dedicated to the presence of laminar zones which, at model scale, can have a significant extension on the blade area. For this specific purpose, in addition to the standard SST k-ω turbulence model, the Gamma-Re-Theta transition model was tested. The transition model provided a reasonable representation of the laminar zones on the blades, and it performed equally well, with respect to the fully turbulent SST model, in predicting the performances of propellers, as shown in Figure 21 when compared against model test data. It was then decided to use the transition model for all the following simulations at model scale conditions, keeping in mind its limitation, that it is a correlation-based model, where reliable correlations are available, and in quite limited volume, for single propellers only.

For the same design, three different values of RPM ratio were investigated, specifically the speed of rotation of the FWD propeller was kept unchanged while the rpm of the AFT propeller was increased or decreased so that the ratio n_{AFT}/n_{FWD} was ± 10% of the design value, as previously described in Section 4.2.

In the Figure 22 the CFD results for all the three rpm ratios are compared against the model test data as obtained for the basic SOBC-1 design in the SINTEF Ocean Towing Tank. The agreement is very satisfying both in terms of characteristics of the propellers operating as a CRP unit, and in terms of total characteristics of the unit. The same trend observed in model tests (see Figure 5), was confirmed in the CFD simulations.

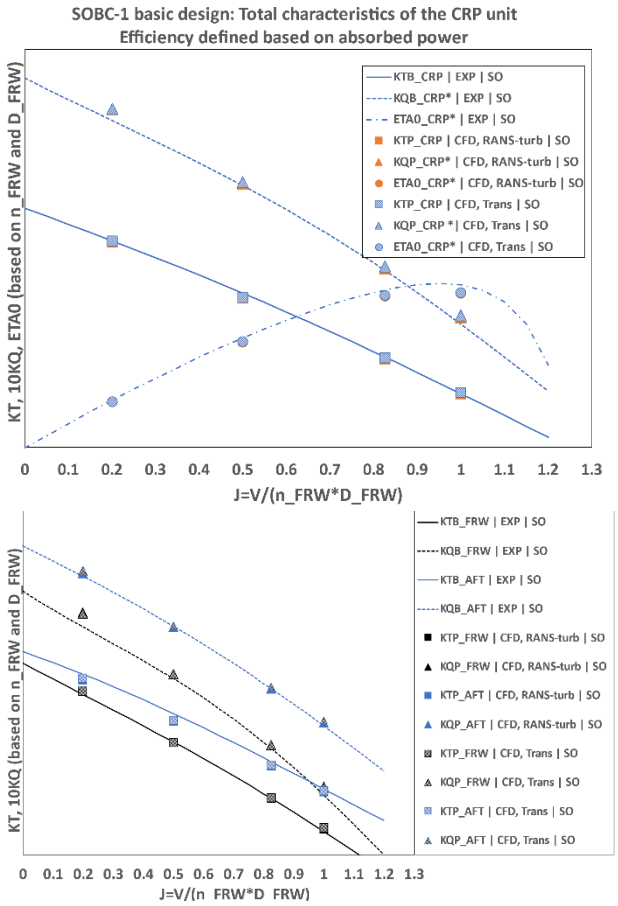

Figure 21 Basic SOBC-1 design. Comparison of CFD results, with fully turbulent and transition models, against model test data (SINTEF Ocean).

5.2.3 New design

Some larger discrepancies between CFD results and experimental data, specifically on the thrust and torque of the AFT propeller, were experienced in some cases where more extreme design solutions were considered. In Figure 23, both thrust and torque on the AFT propeller are overpredicted, for a new design, here called D-1, with C_{TH}=4.0, where the load is evenly balanced between the front and aft propeller. This overprediction appears to be larger than what was observed in previous cases, like the basic SOBC-1 design, as previously shown in Figure 21. In the basic SOBC-1 design, the load distribution is more unbalanced toward the AFT propeller, which is more loaded than the front one. Although the overprediction on the AFT propeller for D-1, the agreement with model tests data remains satisfying in terms of total characteristics of the CRP unit, as illustrated in Figure 24. Full scale simulations were also carried out for this specific case, and scale effects are clearly visible in the diagrams of both Figure 23 and Figure 24.

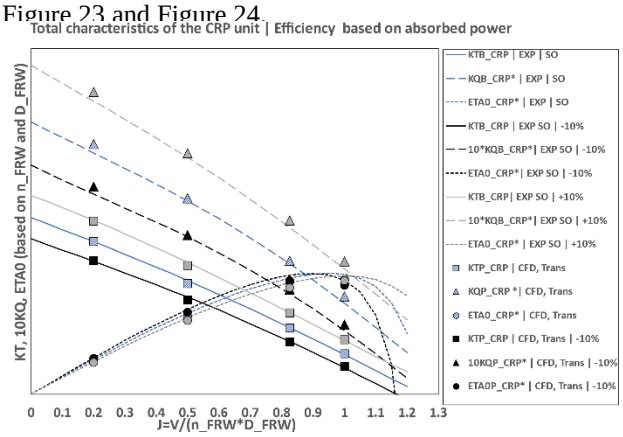

Figure 22 Basic SOBC-1 design. Three rpm ratios. Comparison of CFD results, with transition model,

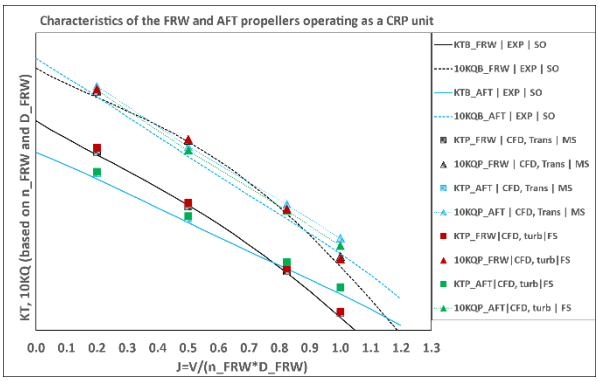

Figure 23 CFD vs. experiments. Overprediction of torque calculated by CFD for the AFT propeller for one specific design (D-1).

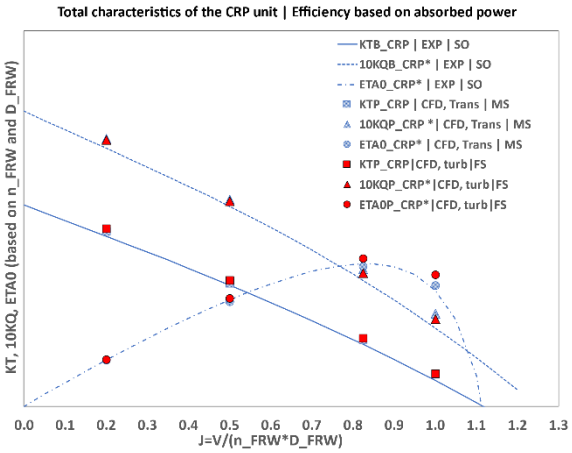

Figure 24 D-1. CFD (MS and FS) vs. experiments. Total characteristics of the CRP unit. Scale effects.

A greater contraction of the front propeller slipstream brings to a significant area of the aft propeller to be outside of the slipstream tube, as illustrated in Figure 25.

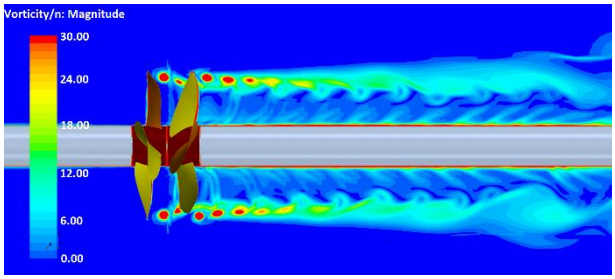

Figure 25 CFD simulations on D-1, J=0.2 Model Scale. Vorticity magnitude contour plot in longitudinal section plane.

The case D-1 is defined by a higher specific thrust than the previous basic design and it is also characterized by a larger blade area ratio, which brings to a reduction of the distance between the blade profiles of the two propellers. This means that the interaction between the propellers is stronger, and the two propellers can influence each other.

A further explanation for the larger deviations between CFD and experiments could be related to the transition turbulent model, which may fail in predicting the extent of laminar zones. At low J values, considerable zones of laminar transition are visible both on the front and rear propeller, as shown in Figure 26. If the levels of turbulence are not correctly modelled, especially on the AFT propeller, it may easily result in too large zones of laminar flow, and hence leading to higher lift of blade sections and increase of both thrust and torque. This would also explain why the full-scale simulations get closer to the measurements.

Figure 26 J=0.2 Laminar zones on FWD and AFT propeller as predicted by the transition turbulent

At high J values such laminar zones are reduced, but it appears that the front propeller operates off-design (at negative angle of attack), as shown in Figure 27 and Figure 28, making the interaction between the two propellers even more complex. All this may contribute to a larger difference between CFD and experimental results.

Overall RANSE methods perform sufficiently well for what concerns integral forces characteristics, also for more extreme designs. In these cases, an accurate prediction of the propeller wake of the front propeller and its interaction with the downstream propeller would be necessary to have a better prediction also of the integral forces. For this purpose, higher resolution, both spatial and temporal, is needed, together with a more advanced turbulence model, like a scale resolving turbulence model.

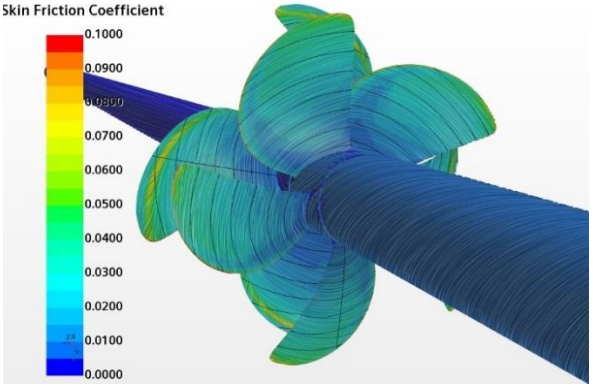

Figure 27 CFD simulations on D-1, J=0.825, MS. Skin friction coefficient and streamlines on the pressure side of FWD and AFT propellers. Negative angle of attach at front propeller.

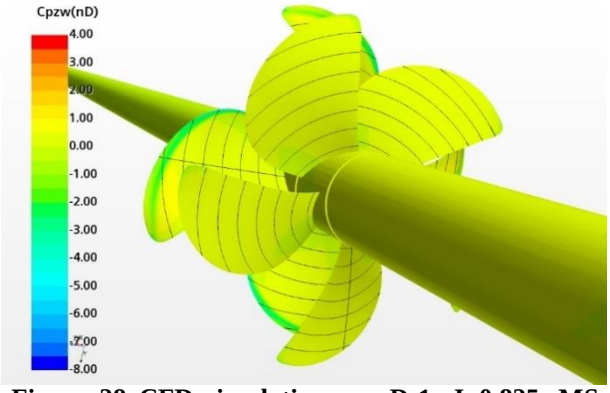

Figure 28 CFD simulations on D-1, J=0.825, MS. Pressure coefficient contour plot on the pressure side of FWD and AFT propellers. Negative angle of attach at front propeller.

5.2.4 Variation of blade area ratio

Another investigation was performed, by CFD only, at full scale, by changing the blade area ratio of both FWD and AFT propellers, while keeping the same pitch setting and the same rpm ratio between front and aft propeller, as illustrated in Figure 29.

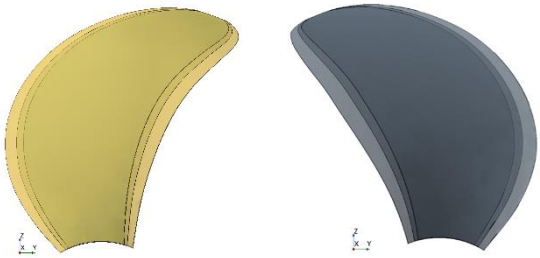

FWD AFT

Figure 29 Three different area ratio blade models for the FWD and AFT propellers of the CRP unit

The open water characteristics, obtained for the three designs, are reported in Figure 30 and Figure 31 for the FWD and AFT propeller respectively, operating as CRP unit, and in Figure 32 in terms of total characteristics of the

CRP unit. No model tests were performed in this case, and CFD simulations were used to provide the OW curves to fill the propeller series matrix. Additional J values (J=1.1 and 1.2) were simulated, to better represent the higher efficiency working conditions. From the simulation points, 4th order polynomials were obtained for the thrust, torque and efficiency, for the single propellers and for the unit, so that the performances of the CRP unit can be calculated for any loading, as for example at J=1.3 as shown in Figure 32.

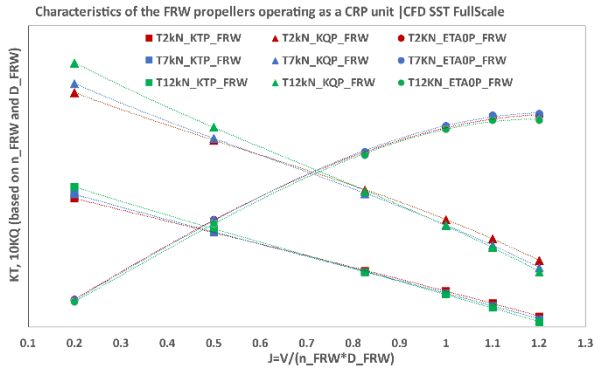

Figure 30 CFD simulations, Full-scale. FWD propeller operating in a CRP unit. Three different area blade models.

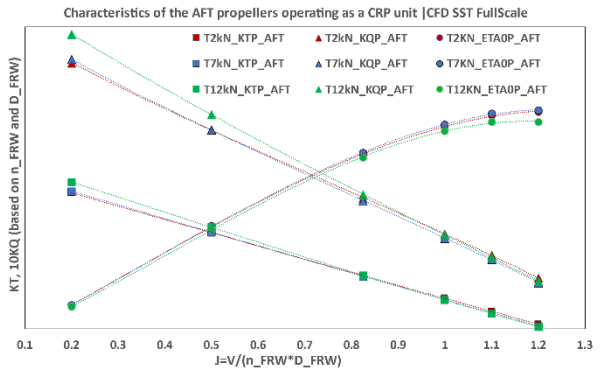

Figure 31 CFD simulations, Full-scale. AFT propeller operating in a CRP unit. Three different area blade models.

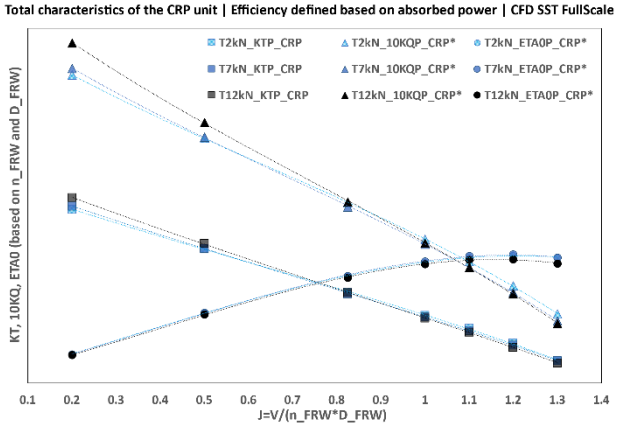

Figure 32 CFD simulations, Full-scale. Total characteristics of the CRP unit. Three different area blade models.

The same diagram with open water CFD results of the CRP unit can be presented as function of propeller loading coefficient C_{TH}. The same trend observed in Figure 6 for the experimental data is shown in Figure 33 for the CFD results. From the diagrams it appears that the design with the largest blade area has the lowest efficiency at design condition, while presenting the largest thrust and torque at heavy loading. This is maybe due to the fact that the pitch setting remains unchanged while modifying the blade area. The propeller with the largest blade area is experiencing, on a large portion of the blade, flow conditions for which it was not designed. Changing the blade area without modifying the pitch setting makes this propeller model less efficient than the others, demonstrating the importance of a good design.

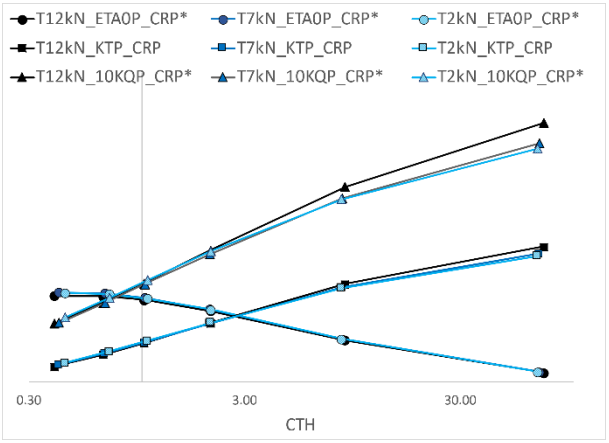

Figure 33 CFD simulations, Full-scale. Total characteristics of the CRP unit. Three different area blade models.

6 MAIN FINDINGS AND CONCLUSIONS

The series provides an energy efficient alternative to the conventional open and ducted propellers for a wide range of propeller loading coefficients.

Experimental results were compared showing good agreement when the same method and similar set up is used. This also includes the comparison of the test results at SINTEF Ocean and SVA Potsdam, which additionally verifies the usability of the measured open water curve as reference for the numerical investigations.

The potential flow code provides a fast tool for evaluating the performance of the contrarotating propellers; however, the complexity of the flow leads to higher deviation than CFD compared to model experiments. The deviations are higher for high thrust loading coefficients as well as for low distances of the propellers to each other. The deviations seem not to be explainable only by the relative distance *x*/*D* and the thrust loading coefficients, but also by the absolute distance of the 3D blade contours of both propellers when moving past each other. For high pitches and large area ratios, the absolute distance decreases compared to propellers with low area ratio and low pitch having the same relative distance *x*/*D*. Since the propeller wake is modeled (pitch and shape) in potential flow theory, small

distances and high loadings lead to the fact that both propellers influence their wake additionally to their global and iteratively covered influence on each other. Thus, the induced velocities presumably develop differently to the assumptions of the potential flow codes when the conditions are extreme. Since both propellers and wake surfaces are not modelled and solved in one single system in the present case, it is impossible to include this influence with something other than corrections. These corrections need the knowledge about representative measured or CFD calculated reference cases.

CFD analyses show for most cases good agreement with model test results, though some deviation is noticed for extreme designs, showing the complex physics and flow of contrarotating propellers. CFD analyses provided invaluable insight in the detail of flow around the propellers and interaction between the fore and rear propellers, allowing for optimization of the series.

Cavitation tests provide insight into the interaction between the fore and aft propellers on the cavitation performance of the contrarotating propeller set. For the presented case study in the cavitation tunnel, the design point of the propeller shows an excellent cavitation behavior. For lower cavitation numbers, the aft propeller diameter should be decreased slightly. The dissipation of the tip vortices due to the contrarotating propellers is a positive detail to mention.

ACKNOWLEDGMENTS

The work presented in this paper has been conducted within the framework of the research and innovation project “Brunvoll Contra Rotating Propeller on single shaft line for main propulsion” (RCN project number 317775) with funding from the Research Council of Norway and Brunvoll. The support received from the Research Council of Norway and Brunvoll is greatly appreciated.

REFERENCES

Beveridge, J. L. (1974). ”Thrust deduction in Contra Rotating Propellers”
NSRDC Report 4332

Bjärne, E. (1973). ”Systematic studies of contra-rotating propellers for merchant ships”
Proc. IMAS 73, London 4-8 June 1973

Breslin, S. and Andersen, P. (1994). ”Hydrodynamics of Ship Propellers”
Cambridge: Cambridge University Press

ITTC (2017a). "Guideline Hybrid Contra-Rotating Shaft Pod Propulsors Model Test" ITTC – Recommended Procedures and Guidelines.

ITTC (2017b). "Model – Scale Cavitation Test "
ITTC – Recommended Procedures and Guidelines.

Kracht, A., Nolte A. (1971). ”Modellversuche für gegenläufige Propeller (VWS, HSVA)”
FDS Bericht 20/1971

Kracht, A. (1976). ”Experimentelle Untersuchung der Schub- und Drehmomentverhältnisse bei kontrarotierenden Propellern
VWS-Bericht Nr. 749/76, FDS-Bericht 56/

Kracht, A. (2000). ”Gegenläufige Propeller”
Handbuch der Werften, Band XXV

van Lammeren, W.P.A., van Manen, J.D., Oosterveld, M.W.C. (1969). “The Wageningen B-Screw series.” *Trans. SNAME*.

van Manen, J. D., Sentic, A. (1956). ”Contra-rotating Propellers”
International Shipbuilding Progress, vol. 3, no. 25, pp. 459-473

van Manen, J. D., Oosterveld, M. W. C. (1968). ”Model tests on contra-rotating propellers”
International Shipbuilding Progress 15, No. 172

Nouri M. N. et al. (2018). “Optimization of a marine contra-rotating propellers set“. Ocean Engineering, Vol. 167, Novemeber 2018, pages 397-404

Oosterveld, M. W. C. (1971). ”Investigations on different propeller types”
International Shipbuilding Progress vol. 18, no. 198, pp. 32-55

Oosterveld, M.W.C., van Oossanen, P. (1975). “Further computer-analysed data of the Wageningen B-screw series” International Shipbuilding Progress vol. 22, no. 251, pp. 251-262

Paik, K-J et al. (2015). “Investigation on the wake evolution of contra-rotating propeller using RANS computation and SPIV measurement“. IJNAOE, Vol. 7, Issue 3, May 2015, pages 595-609

Schmidt, D. (2000). ”Systematische Untersuchungen zur Klärung des Einflusses des Propellerabstandes, der Gondelabmessungen und des Drehzahlverhältnisses eines Contra-Rotating-Twin-Propellers”
Bericht 2452, Schiffbau-Versuchsanstalt Potsdam

Schulze, R. (1997). “Globale Optimierung von Propellern, Jahrbuch der Schiffbautechnischen Gesellschaft“ Band 91, S. 97-104, Springer-Verlag Berlin Heidelberg New York

Schulze, R. (2019). “Design strategies for noise optimized propellers for multiple screw ships“
Jahrbuch der Schiffbautechnischen Gesellschaft, 113. Band 2019, Hamburg, ISBN 978-3-87700-146-2, Schiffahrts-Verlag „Hansa“ GmbH & Co. KG